Robotica (2008) volume 26, pp. 9–17. © 2007 Cambridge University Press
doi:10.1017/S0263574707003542 Printed in the United Kingdom

Disturbance rejection by online ZMP compensation

Vadakkepat Prahlad,* Goswami Dip and Chia Meng-Hwee

Department of Electrical and Computer Engineering, National University of Singapore, Singapore 117576

(Received in Final Form: May 8, 2007. First published online: June 25, 2007)

SUMMARY

A novel method of Zero-Moment-Point (ZMP) compensation is proposed to improve the stability of locomotion of a biped, which is subjected to disturbances. A compensating torque is injected into the ankle-joint of the foot of the robot to improve stability. The value of the compensating torque is computed from the reading of the force sensors located at the four corners of each foot. The effectiveness of the method is verified on a humanoid robot, MANUS-I. With the compensation technique, the robot successfully rejected disturbances in different forms. It carried an additional weight of 390 gm (17% of body weight) while walking. Also, it walked up a 10° slope and walked down a 3° slope.

KEYWORDS: Biped locomotion; Humanoid; Zero-Moment-Point compensation.

1. Introduction

Humans have always been fascinated by humanoid robots—robots that look and function like humans. A particular area of research interest, currently being pursued actively in humanoid robotics, is the control of biped locomotion.

The main motivation in the research on bipedal locomotion is its much-needed mobility required for maneuvering in environments meant for humans or in rugged terrains. Wheeled vehicles can only move efficiently on relatively flat terrains, whereas a legged robot can make use of suitable footholds to traverse in a rugged terrain. Bipedal walking is a much less stable activity than say four-legged walking, as multilegged robots have more footholds for support. Bipedal walking allows instead greater maneuverability, especially in smaller areas.

Even though bipedal walking occurs to humans as a trivial task, it is a complex balancing act for a robot to even walk on flat ground. Thus, much research has been done on algorithms and methods to control bipedal locomotion. The traditional approach[13,15–17] is the generation of walking gaits by means of generating joint-trajectories and controlling each joint for trajectory-tracking so as to mimic human walking.

The trajectory-based control is inefficient in energy usage.[4,6] The joints are encumbered by motors and high-reduction gearing, making joint movements inefficient when the actuators are switched on and nearly impossible when they are switched off. Nevertheless, these control techniques are still versatile and successful in biped locomotion.

* Corresponding author. E-mail: prahlad@ieee.org

In direct contrast to trajectory-based control, passive dynamic walking pioneered by McGeer[1,2] is another approach towards bipedal walking. Passive dynamic walkers make use of inherent dynamics of the mechanism to generate stable periodic walking motions.[3,4] Collins[5] successfully built the world's first 3D passive-dynamic walker that can walk down a 3° slope without any actuation. Subsequently, the group developed a minimally powered version of the passive-dynamic walker (Cornell biped).[6]

Biologically-inspired bipedal locomotion control is yet another popular area currently under research. There exist intra-spinal neural circuits capable of producing syncopated oscillatory outputs controlling the walking pattern in vertebrates.[7] These neural circuits are often termed neural oscillators or Central Pattern Generator (CPG). Complete quadrupedal stepping[8], for example, in a cat can be generated on a flat horizontal surface, when a section of its midbrain is electrically stimulated. Nakanishi *et al.*[9] used learning for bipedal locomotion. Morimoto *et al.*[10] used reinforcement learning adaptation for walking down the slope, which was implemented on a 5-link biped model.

In trajectory-based control, one major criterion in the generation of joint trajectories is the position of the Zero-Moment Point (ZMP). ZMP is defined as the point on the ground where the net moment of the inertial forces and the gravity forces has no component along the horizontal axes.[11] For stable dynamic locomotion, the necessary and sufficient condition is to have the ZMP within the support polygon at all stages of the locomotion gait. The support polygon is the area on the ground covered by the feet during locomotion.

Based on the ZMP criterion, various algorithms of trajectory planning have been suggested. Most of these algorithms involve the calculation of the desired joint trajectories via inverse kinematics to satisfy the ZMP criterion and the calculation of various joint torques needed. One such approach is to specify a desired hip trajectory while satisfying the ZMP criterion.[12,13] Successful examples of such techniques include Manus-I[14] and the Honda Asimo Robot.[15]

ZMP compensation is an approach to alter joint trajectories or joint torques to enable the robot to react to the disturbances from the environment by keeping the ZMP within the support polygon. In Kim *et al.*,[12] a constant compensation procedure is discussed. The reference angles to the ankle roll and pitch joints are changed by a constant amount when the ZMP moves out of an area in the support polygon. In Honda Robot,[15] ZMP compensation is done by revising the prescribed ZMP during walking when there is deviation from

the desired ZMP. The problem of walking on uneven terrain is addressed in this work. In ref. 16, a stable walking pattern generation problem is addressed by ZMP compensation. The ZMP compensation is done by the trunk motion while walking on a flat surface. In ref. 17, ZMP compensation is done by whole-body-motion control for stable walking pattern generation. In Mitobe *et al.*,[18] the ground reaction forces and cartesian coordinates of the robot are measured and a feedback is given to control the position of the robot by manipulating the position of the ZMP. The control mechanism involves very precise control of the joint-angular position of the robot, which needs high-gain-feedback. In this work, mainly the smoothness of the walking gait of the robot is considered. Kajita *et al.*[19] introduced preview control where ZMP compensation problem is addressed as a servo problem. The effectiveness of the method is verified in simulation while the robot is walking on a spiral path. In ref. 20, simulation study of ZMP compensation by modifying the trajectories of the different joints is done for walking on a flat surface.

In the conventional ZMP tracking or compensation problem, the independent joint-actuator controllers need to be accurate to provide the exact amount of torque to the actuators. Therefore, the joint controllers require high-gain-feedback control by using high-ratio reduction gear. This makes the robotic system slower, heavier, and more expensive. The conventional ZMP compensation methods mainly address small disturbances due to uneven terrain or oscillation.

The physical implementation of a trajectory-based compensation technique is examined on Manus-I in this work. Manus-I has 12 degrees of freedom (DOF) in the lower body, and each joint is driven by an radio-controlled servo motor [www.hitecrcd.com/homepage/product-fs.htm]. A Digital Signal Processor (DSP) (Motorola 56F807) controls walking motion of the robot by sending the desired joint trajectory signals to various leg joint motors. The ZMP at each instant is measured using force sensors located at the corners of each foot bottom. The DSP controller receives and processes the data from the force sensors. Compensation for the ankle reference angles is calculated according to the deviation of the ZMP.

The biped model, the force sensors, and the method to measure ZMP are discussed in Section 2. The online ZMP compensation technique for disturbance rejection is discussed in Section 3. The compensation technique is used for the stabilization of the biped locomotion while walking on a flat terrain, walking up/down the slope, carrying weight, and experiencing sudden push from front or back. Section 4 discusses about the four different applications of the compensation method in biped locomotion. The paper is concluded in Section 5.

2. Measurement of ZMP of the Robot

2.1. Biped model

The biped model considered in this work has six DOF in each leg: two DOF at ankle, one DOF at knee, and three DOF at hip. The biped model has the mass distribution as shown in Fig. 1. The masses of the links are considered as point-mass because they are made of very light-weight material with motor-weight being the dominant part. The mass of the upper body is also considered as point-mass and taken into account by the mass m_2. The values of the parameters of the robot model (Fig. 1) are shown in Table I. The model of the bipedal lower part of the Humanoid MANUS-I is developed in visualNastran 4D simulation environment (Fig. 2). The real robot is shown in Fig. 3.

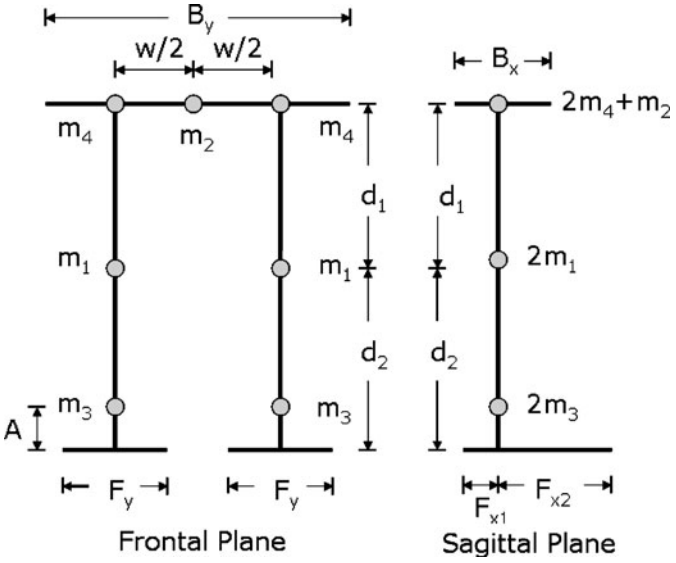

Fig. 1. Biped model in the frontal and sagittal plane.

2.2. Force sensors

Tekscan FlexiForce force sensors are used to measure the forces acting on the feet of the robot. An illustration of the mechanical installation of the force sensors is provided in Fig. 4. The electrical resistance of the force sensors (R_F) are inversely proportional to the magnitude of the normal force acting on the force sensors. A simple electrical circuit (Fig. 5) converts the force measured into voltage by Eq. (1) [www.tekscan.com/pdfs/Flexiforce UserManual.pdf]

$$R_F = \frac{\vartheta}{\text{Force}}$$

Table I. Parameters of the biped model.

Parameters	Values
m_1	0.07 Kg
m_2	1.52 Kg
m_3	0.14 Kg
m_4	0.21 Kg
d_1	0.15 meter
d_2	0.12 meter
w	0.06 meter
A	0.002 meter
B_x	0.1 meter
B_y	0.14 meter
F_{x1}	0.045 meter
F_{x2}	0.08 meter
F_y	0.055 meter

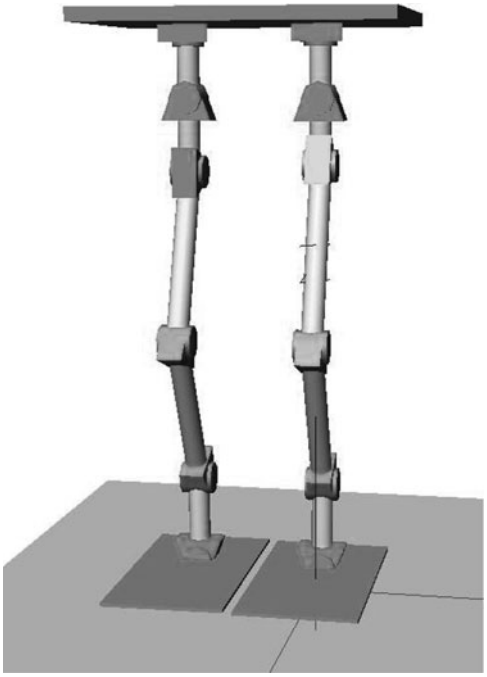

Fig. 2. Biped model of MANUS-I in visualNastran 4D environment.

Fig. 3. MANUS-I.

$$V_{adc} = \left(\frac{390K\Omega}{R_F + 390K\Omega} \right) \times V_{ref} \qquad (1)$$

where ϑ is the calibration constant, $V_{ref} = 5$ V and V_{adc} is the voltage measured by the analog-to-digital converter of the DSP.

The positions of the force sensors at the bottom of the feet of the robot, are illustrated in Figs. 6 and 7. f_i's and

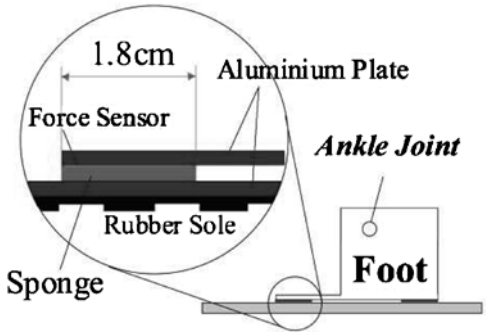

Fig. 4. Mechanical installation of force sensors.

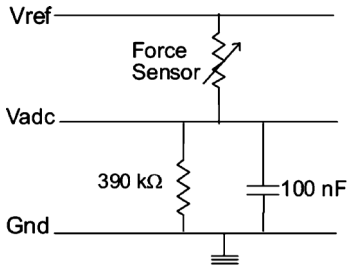

Fig. 5. Force-to-Voltage converter circuit.

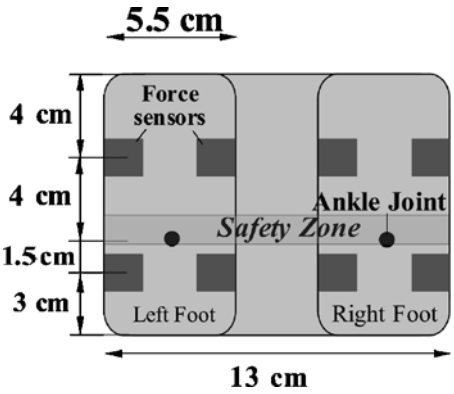

Fig. 6. Positions of the foot sensors at the bottom of the feet.

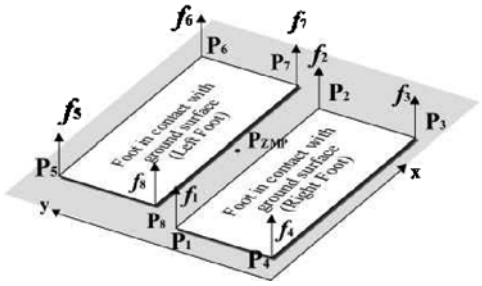

Fig. 7. Reading of the force sensors.

P_i's represent, respectively, the readings and positions of the eight force sensors.

2.3. Measurement of ZMP

The center of pressure (COP) is defined as the point on the ground where the resultant of the ground-reaction force acts. When the ZMP is within the support polygon, the COP coincides with ZMP.[22] Therefore, the measurement of ZMP is dependent on how the contact points are modeled. In

ref. 21, one ZMP sensor is devised, which models the contact between the biped's feet and the ground as a collection of infinite points. The pressure, sensed by the ZMP sensor, is distributed. Force, sensed in each contact point, is measured by a voltage generated by an equivalent electrical circuit. In our work, the contact points are four instead of infinite, while the principle of ZMP computation is same as in ref. 21. This makes the computational and implementation effort considerably less with a little compromise in accuracy.

During walking, when one leg is swinging, the mass of the whole body can be replaced by the total mass of the robot located at the center of mass (CM) of the robot as point-mass and is connected to the foot at stance like an inverted pendulum. The simplified model shown in Fig. 8 is used to approximate the biped model in the rest of the paper. In Fig. 8, "c" is the CM of the robot with one leg swinging and "a" is the ankle-joint of the other leg, which is on the ground; x_i and y_i $(i = 1, 2)$ are the positions of the force sensors in x and y directions, in sagittal and frontal plane, respectively; l is the distance of the CM from ankle-joint in sagittal plane; L is the distance of ZMP from the ankle joint. l can be considered as a link with concentrated point-mass at the end. ϕ is the angle between the link and the z-axis; α is the angle between L and the z-axis; τ is the torque at the ankle-joint about y-axis; F_{ext} is the disturbance force applied to the robot as disturbance; m is the total mass of the robot; and g is the gravitational acceleration. The motions in the sagittal plane and frontal plane are considered separately because the motions in these two planes are weakly coupled.[23] The ZMP in x-direction is calculated from the motion in sagittal plane by Eq. (2)

$$F_1(x_1 - x_{zmp}) - F_2(x_2 + x_{zmp}) = 0$$
$$\Longrightarrow x_{zmp} = \frac{F_1 x_1 - F_2 x_2}{F_1 + F_2} \tag{2}$$

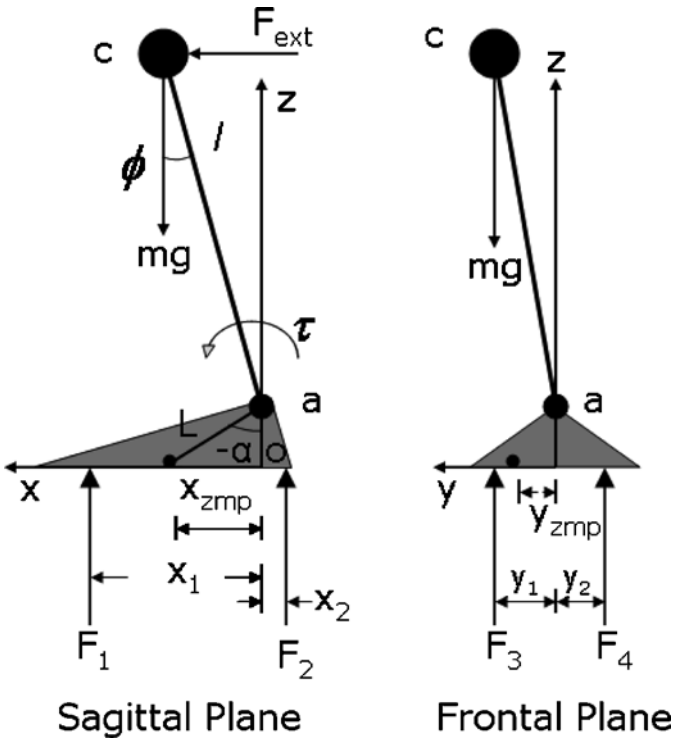

Fig. 8. Simplified model of the biped in sagittal and frontal plane.

where $F_1 = f_2 + f_3$ or $F_1 = f_6 + f_7$ and $F_2 = f_1 + f_4$ or $F_2 = f_5 + f_8$, when the right leg or the left leg is on the ground, $x_1 = 4$ cm, $x_2 = 1.5$ cm (Figs. 6 and 7). The ZMP in y-direction is calculated from the motion in frontal plane by Eq. (3)

$$F_3(y_1 - y_{zmp}) - F_4(y_2 + y_{zmp}) = 0$$
$$\Longrightarrow y_{zmp} = \frac{F_3 y_1 - F_4 y_2}{F_3 + F_4} \tag{3}$$

where $F_3 = f_1 + f_2$ or $F_3 = f_6 + f_5$ and $F_4 = f_3 + f_4$ or $F_4 = f_7 + f_8$, when the right leg or the left leg is on the ground, $y_1 = y_2 = 2.75$ cm (Figs. 6 and 7).

3. Online ZMP Compensation

The compensation technique proposed in this work mainly focuses on the sagittal plane motion. The method can also be extended for the frontal plane motion. Computationally, the compensation is done based on the following assumptions:

A1: The motion of the biped is confined to the sagittal plane.

A2: It is assumed that the compensation torque $\Delta\tau$ causes change in acceleration of the compensating link, $\Delta\ddot{\phi}$, while link-velocities do not change due to the action of $\Delta\tau$, $\Delta\dot{\phi} \approx 0$. The physical significance of this assumption is that the biped's movements are slow enough to neglect the effects of the coriolis ($\dot{\phi}\Delta\dot{\phi}$) and the centrifugal ($(\Delta\dot{\phi})^2$) forces.

A3: It is assumed that when the biped is on the move, the ZMP is always within the support polygon. This assumption ensures that during walking, when one leg is swinging, the other foot is in contact with the ground without any foot rotation.

A4: It is assumed that the value of l is constant and almost equal to the height of the CM during walking, as x and y components of the CM are much less compared to the z-component of the CM, which leads to $l \approx 0.1$ m for MANUS-I.

A5: $|\ \frac{L}{l}\cos(\phi + \alpha)\ | \ll 1$ in (10). As the height of the ankle-joint is smaller compared to the height of CM, $0 < L/l < 1$ and $|\ \cos(\phi + \alpha)\ | < 1$. When $0 < L/l \ll 1$, i.e., x_{zmp} is close to the ankle-joint, $|\ L/l\cos(\phi + \alpha)\ | \ll 1$. When the value of L/l is relatively high, i.e., x_{zmp} is far from the ankle-joint, α is larger which means $\cos(\phi + \alpha)$ is small leading to $|\ L/l\cos(\phi + \alpha)\ | \ll 1$.

A6: The amount of disturbance, which is rejected, is restricted by the torque rating of the motor. It is assumed that the disturbances are applied gradually, and that the torque requirement at the ankle actuator does not exceed the torque-rating of the ankle actuators.

A7: When the value of x-ZMP is within a closer range of ankle-joint (0.25 to 0.5 of the normalized foot-length), then the disturbance is assumed to be zero. This range is referred to as "safety zone." When the x-ZMP value is beyond the specified range, it is assumed that the disturbance is acting on the robot. The disturbance can be both due to the external forces (if any) and due to the shifting of robot's weight during walking.

Let, at the $(k-1)$th sampling interval, the x-ZMP position is x_{zmp}, which is within the "safety zone." The moment about x_{zmp} during $(k-1)$th sampling interval is given by

$$M_{zmp}^{k-1} = F_1(x_1 - x_{zmp}) - F_2(x_2 + x_{zmp}) = 0. \tag{4}$$

When a disturbance force (F_{ext}) is acting on the robot in x-direction and compensation is not applied, at kth sampling interval the moment about x_{zmp} is computed using (2) and (4)

$$\begin{aligned} M_{zmp}^{k} &= (F_1 + \Delta F_1)(x_1 - x_{zmp}) - (F_2 + \Delta F_2)(x_2 + x_{zmp}) \\ &= \Delta F_1(x_1 - x_{zmp}) - \Delta F_2(x_2 + x_{zmp}) \\ &= \Delta F_1 x_1 - \Delta F_2 x_2 - (\Delta F_1 + \Delta F_2)x_{zmp} \\ &= \Delta F_1 x_1 - \Delta F_2 x_2 - \frac{(\Delta F_1 + \Delta F_2)}{F_1 + F_2}(F_1 x_1 - F_2 x_2). \end{aligned} \tag{5}$$

The values of ΔF_1 and ΔF_2 are measured from the changes in the force sensor reading between successive sampling intervals. Therefore, the value of M_{zmp}^{k} is measurable. The system is equivalent to a two-link planner manipulator with joints located at x_{zmp} and "a." The length of the two links are "L" and "l." The torques τ and M_{zmp}^{k} are acting at the two joints, which are located at x_{zmp} and "a," respectively (Fig. 8).

Dynamics of the above two-link robotic system is computed by Lagrangian formulation.[22] Without compensation, ankle-joint torques τ and M_{zmp}^{k} are given by

$$\begin{aligned} \tau &= J\ddot{\phi} + mlg\sin(\phi) + F_{ext}l\cos(\phi), \\ M_{zmp}^{k} &= (J + mlL\cos(\phi + \alpha))\ddot{\phi} \\ &\quad + mlg\cos(\phi) + mLg\sin(\alpha), \end{aligned} \tag{6}$$

where J is the moment of inertia of the robot about y-axis of the ankle-joint, i.e., $J = ml^2$. If there is no compensation provided, the ZMP will shift. The shift in ZMP value can be calculated from the force sensor readings with the same method discussed in Section 2.3. Without compensation, the x-ZMP value shifts by an amount

$$\Delta x_{zmp} = \frac{M_{zmp}^{k}}{F_1 + F_2 + \Delta F_1 + \Delta F_2}. \tag{7}$$

The compensation acts only if $(x_{zmp} + \Delta x_{zmp})$ goes beyond the designated safety zone. Let, $\Delta\tau$ be the compensation torque applied at the ankle-joint during kth sampling interval, which makes the moment about x_{zmp} zero. The system is equivalent to a two-link planner manipulator with a zero torque at x_{zmp} and $(\tau + \Delta\tau)$ acting at ankle-joint "a." With the assumption A2, the system dynamics is given by

$$\begin{aligned} \tau + \Delta\tau &= J(\ddot{\phi} + \Delta\ddot{\phi}) + mlg\sin(\phi) + F_{ext}l\cos(\phi), \\ 0 &= (J + mlL\cos(\phi + \alpha))(\ddot{\phi} + \Delta\ddot{\phi}) \\ &\quad + mlg\cos(\phi) + mLg\sin(\alpha). \end{aligned} \tag{8}$$

Therefore, the compensation torque $\Delta\tau$ is computed from (6) and (8)

$$\begin{aligned} \frac{\Delta\tau}{M_{zmp}^{k}} &= -\frac{J}{J + mlL\cos(\phi + \alpha)} \\ \Longrightarrow \Delta\tau &= -\frac{M_{zmp}^{k}}{1 + \dfrac{mlL\cos(\phi + \alpha)}{J}}. \end{aligned} \tag{9}$$

Considering the assumption A5, it is claimed that

$$\begin{aligned} \Delta\tau &= -\frac{M_{zmp}^{k}}{1 + \dfrac{mlL\cos(\phi + \alpha)}{ml^2}} \\ &= -\frac{M_{zmp}^{k}}{1 + \dfrac{L}{l}\cos(\phi + \alpha)} \\ &\Longrightarrow \Delta\tau \approx -M_{zmp}^{k}. \end{aligned} \tag{10}$$

Thus, the compensation torque $\Delta\tau$, which is required at the ankle-pitch joint, is computed from the force sensors reading. The required torque is provided by proper adjustment of ϕ by changing the ankle-pitch-joint angular position using (6) and (8) as

$$\begin{aligned} \Delta\tau &= -M_{zmp}^{k} = J\Delta\ddot{\phi} = J\frac{\Delta\phi}{(\Delta t)^2} = \eta\Delta\phi, \\ \Delta\phi &= \frac{-M_{zmp}^{k}}{\eta} \end{aligned} \tag{11}$$

where Δt is the sampling interval of the DSP controller and $\eta = J/(\Delta t)^2$ is a constant. $\Delta t = 12.5$ ms for the DSP controller used in this work. The mass of the whole robot is $m = 2(m_3 + m_1 + m_4) + m_2 = 2.36$ Kg. The assumption about m is reasonable as it matches with the weight of the real robot. The numerical values of J and η for MANUS-I are given by

$$\begin{aligned} J &= ml^2 = 0.0236\,\text{kg m}^2, \\ \eta &= \frac{J}{(\Delta t)^2} = 151.04. \end{aligned} \tag{12}$$

The compensation at the ankle-joint's reference angle for disturbance rejection is computed by Eqs. (11) and (12). Similarly, compensation is possible for the disturbances in other forms or directions.

The disturbances are compensated by changing the reference angle of the ankle-pitch joint. The overall block diagram of the ZMP compensation technique is shown in Fig. 9. In Fig. 9, ϕ is the reference position of the ankle-pitch joint without compensation. The reference value of the ankle-pitch-joint servo controller is changed by $\Delta\phi$ amount for disturbance rejection. From the above analysis, it is seen that:

- The proposed ZMP compensation technique is applicable to any bipedal system as long as the system closely follows the assumptions A1–A7.

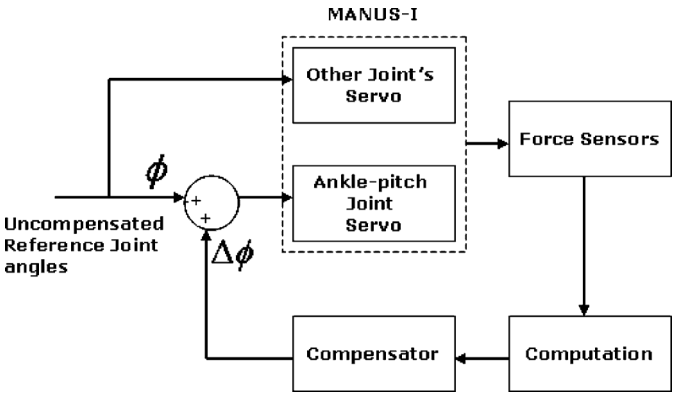

Fig. 9. Block diagram for online ZMP compensation.

- The proposed ZMP compensation technique does not require exact disturbance modeling.
- The torque-rating of the ankle-joint motors decides the maximum amount of disturbance that can be compensated by the above technique. The higher the ankle-joint motor torque-rating is, the higher is the ability to reject disturbances.

In order to evaluate the effectiveness of the compensation technique, it is applied to MANUS-I for disturbance compensation in different applications.

4. Applications, Experiments, and Results

4.1. Improvement of walking on flat surface

x-ZMP positions of the robot are computed from the force measurements while walking on a flat surface using Eq. (2). The x-ZMP value is normalized to the length between the front and back force sensors of the feet. The compensation technique comes into play whenever the x-ZMP position goes beyond the safety zone. The compensation angle at the ankle-joint is calculated using Eqs. (5), (11), and (12). The robot is made to walk on a flat surface without compensation and with compensation over a period of 20 s. Figures 10 and 11

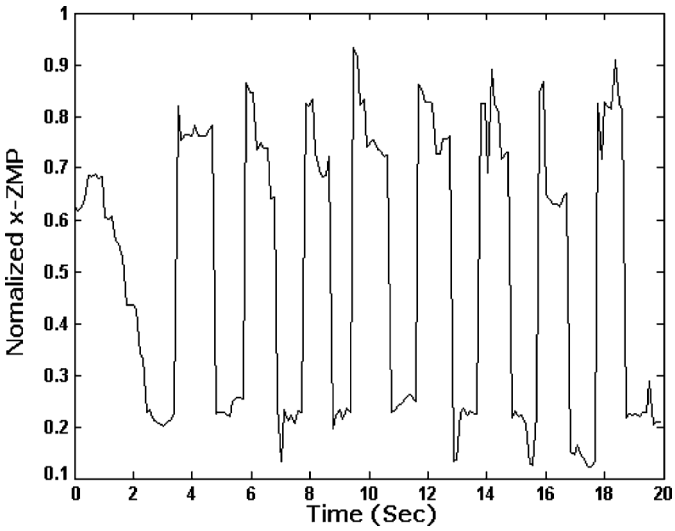

Fig. 10. Normalized x-ZMP Position of Uncompensated Walking Gait.

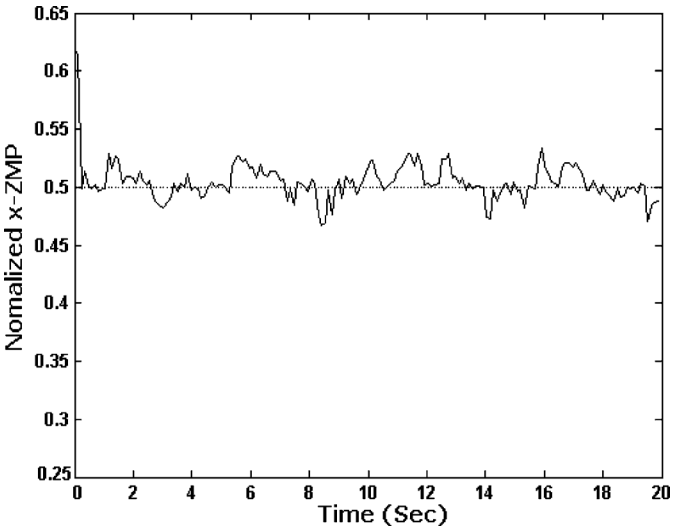

Fig. 11. Normalized x-ZMP Position of Compensated Walking Gait.

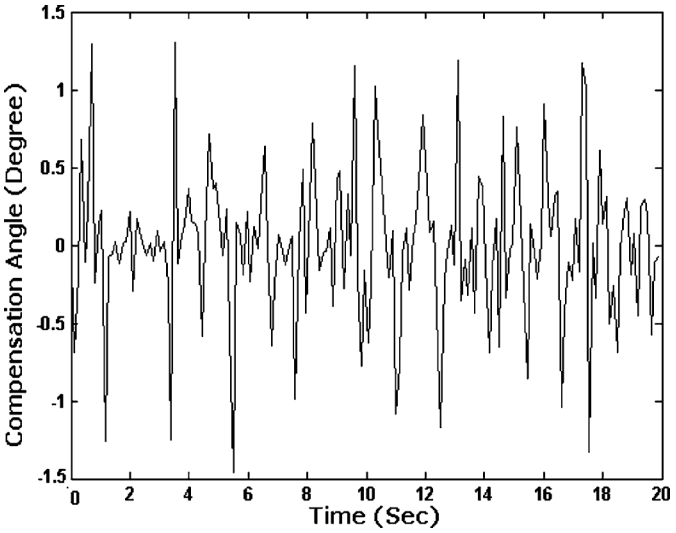

Fig. 12. Compensation at the ankle joint during walking on a flat surface.

show the recorded x-ZMP positions once the walking gait is stabilized starting from a standing position. Figure 12 shows the amount of compensation required at the ankle-pitch joint to keep the x-ZMP position within the safety zone. It is clear from the results that the compensator is able to reduce the magnitude of fluctuation of the ZMP keeping its value within the safety zone.

4.2. Rejecting disturbance due to sudden push

With the compensation at place, the robot's walking gait is more robust to sudden disturbances such as a slight push from behind or from the front. When the robot experiences a push, the ZMP shifts momentarily out of the expected position and goes beyond the safety zone. By ankle-joint compensation, the robot is able to revert back its ZMP position after certain walking cycles, depending on the size of the disturbance. In order to provide a measure of the horizontal force disturbance

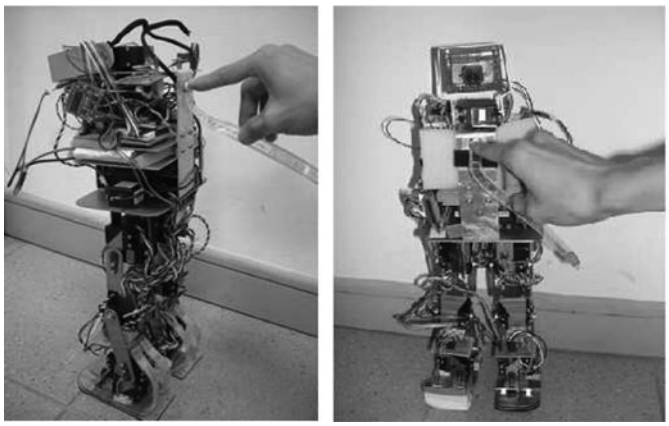

Fig. 13. Measurement of disturbance force.

that the robot can reject, force sensors are attached at the front and back of the robot, 40 cm from the ground (Fig. 13) while the total height of the robot is 50 cm. The force, which is applied to the robot, is measured using an oscilloscope by recording V_{adc} of the force-to-voltage converter circuit (Fig. 5). A short impulse of force is applied to the force sensor over a time period of about 0.5 s in order to measure the maximum force that the robot is able to reject without falling down. A typical oscilloscope display of the force is shown in Fig. 14. Figure 15 shows the normalized x-ZMP position of the robot when it experiences a sudden push of intensity around 3 N from behind. The compensation required at the ankle-pitch joint for rejecting the above disturbance is shown in Fig. 16.

The amount of maximum disturbance, which can be rejected, is dependent on the torque-rating of the ankle-pitch-joint actuator. MANUS-I uses radio-controlled servo motor with torque rating 0.13 Nm at the ankle joints. The maximum forward force (from behind) that the robot can reject is around 3 N while it is able to reject a maximum backward force of around 1.2 N. The walking sequences of the robot with backward and forward disturbances are shown in Figs. 17 and 18, respectively.

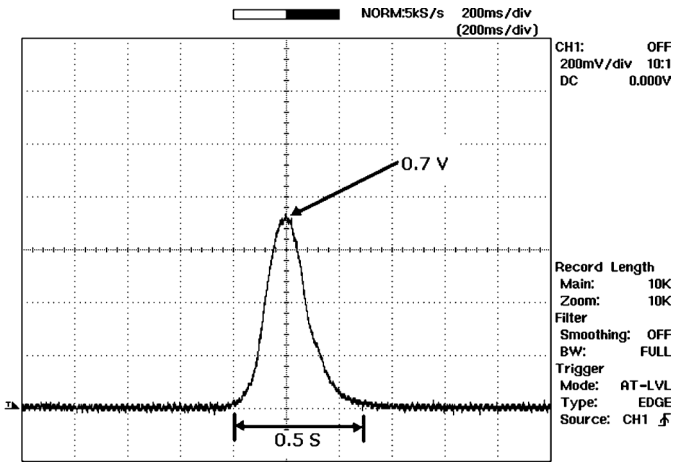

Fig. 14. Oscilloscope display of the applied force.

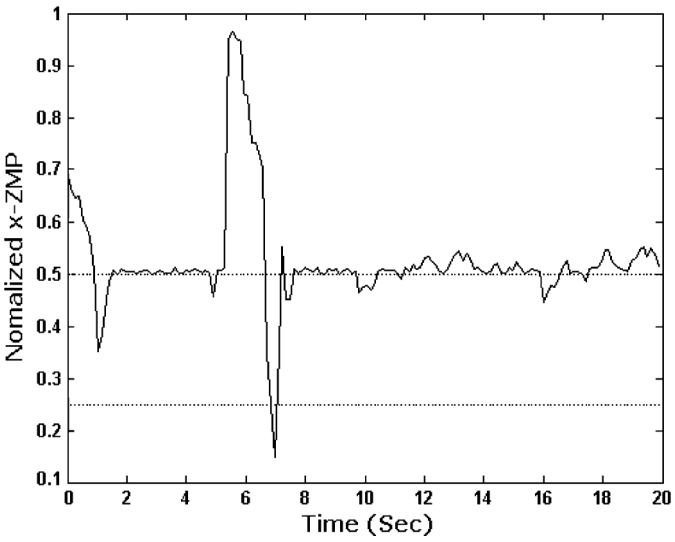

Fig. 15. Normalized x-ZMP Position of MANUS-I when it experience a sudden push of intensity around 3 N from behind.

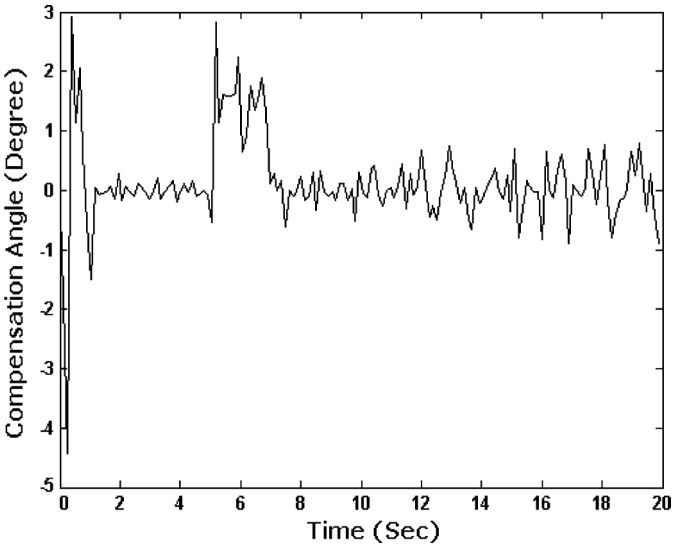

Fig. 16. Compensation at the ankle-joint of MANUS-I to compensate a sudden push of intensity around 3 N from behind.

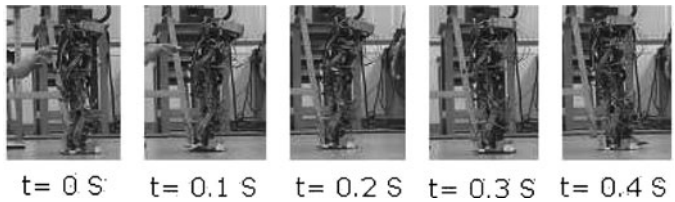

Fig. 17. Robot walking sequence when pushed from behind.

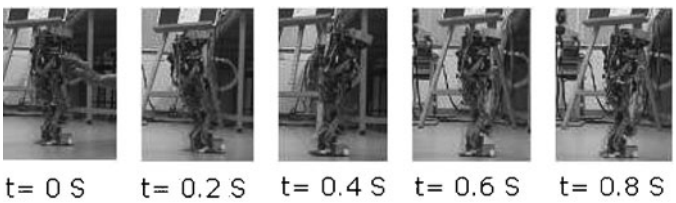

Fig. 18. Robot walking sequence when pushed from the front.

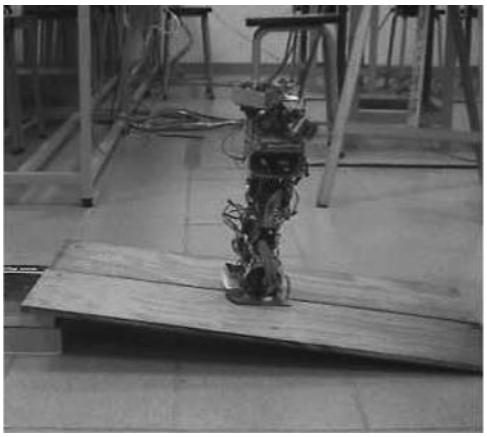

Fig. 19. Walking up a 10° slope.

4.3. Walking up and down a slope

While walking up/down the slope, the compensation angle varies with inclination of the slope. With an increase in slope, the compensation increases. As the compensation angle is changing slowly, the robot adapts to a change in inclination successfully only after about 1 to 2 s depending on the angle of inclination. Due to limitation in ankle-pitch-joint actuator torque-rating, robot is able to walk up a maximum slope of 10° and walk down a maximum slope of 3° on a wooden plank. Figures 19 and 20 show the humanoid, MANUS-I, walking up and down the slope.

4.4. Carrying weight during walking

For walking with additional weight, a basket is attached on the back of Manus-I (Fig. 21). After the compensation technique is applied, the robot is able to carry a maximum of 26 batteries including a metal basket with a total weight of 390 gm and continue walking on a flat surface. The mass of the robot being 2.36 kg, the additional weight is approximately 17% of the robot's weight.

Figure 22 shows the normalized x-ZMP position of the robot while carrying an additional weight of 300 gm at the back for 20 s. The compensation required at the ankle-pitch joint during this period is shown in Fig. 23. As the constant additional weight causes the ZMP to shift, the compensation method adjusts the ankle-pitch angle gradually until the ZMP moves within the safety zone.

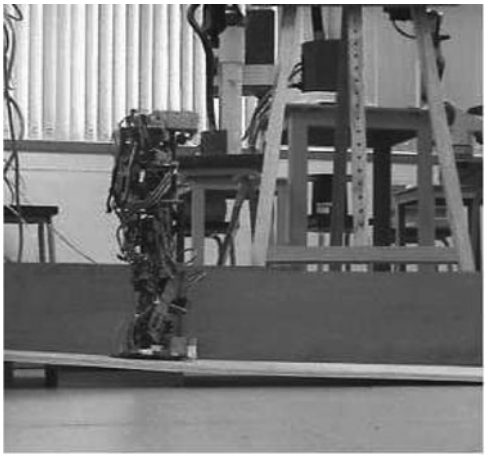

Fig. 20. Walking down a 3° slope.

Fig. 21. Manus-I carrying additional weight.

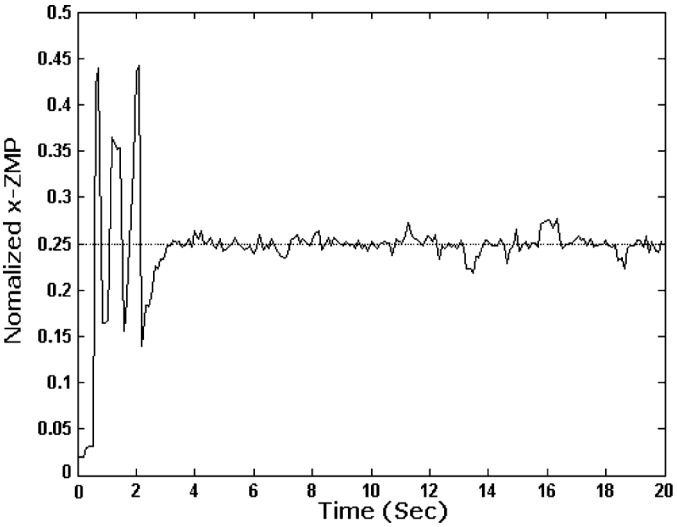

Fig. 22. Normalized x-ZMP position of compensated walking gait while carrying 300 gm weight.

5. Conclusions

One novel online ZMP compensation technique to reject disturbance for improved biped locomotion is proposed and experimentally verified. The proposed compensation method is used in four applications to show its applicability in biped-locomotion-stability improvement and disturbance rejection. In comparison with the existing ZMP compensation methods, the proposed approach is more heuristic in nature as it provides compensation to the reference angles instead of

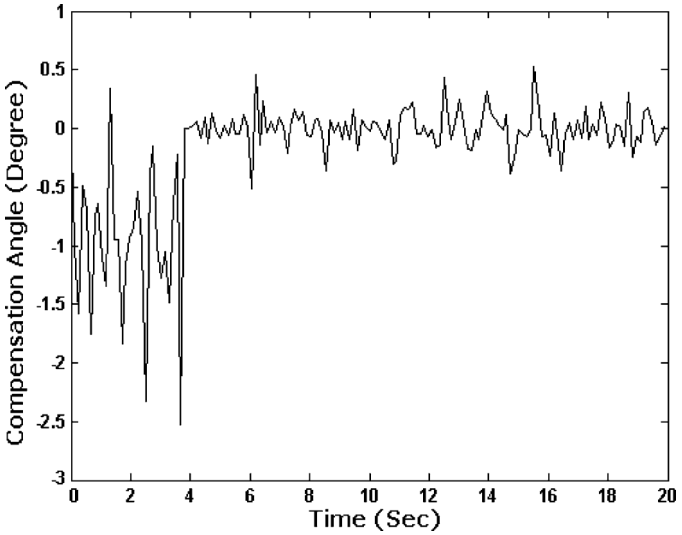

Fig. 23. Compensation at the ankle-joint while carrying 300 gm weight.

changing the desired torque directly. Further investigation is required to provide a more robust performance for such approach in ZMP compensation.

References

1. T. McGeer, "Passive dynamic walking," *Int. J. Robt. Res.* **9**(2), 62–82 (1990).
2. T. McGeer, "Passive Walking with Knees," *Proceedings IEEE International Conference on Robotics and Automation*, Cincinnati, OH (1990), pp. 1640–1645.
3. R. Tedrake, T. W. Zhang, M.-F. Fong and H. S. Seung, "Actuating a Simple 3D Passive Dynamic Walker," *Proceedings of the IEEE International Conference on Robotics and Automation* **5** 4656–4661, (2004).
4. M. Garcia, A. Chatterjee, and A. Ruina, "Efficiency, speed, and scaling of two-dimensional passive-dynamic walking," *Dyn. Stability Syst.* **15**(2), 75–99 (2000).
5. S. H. Collins, M. Wisse and A. Ruina "A three-dimensional passive-dynamic walking robot with two legs and knees," *Int J Robot Res* **20**(2), 607–615 (2001).
6. S. Collins, A. Ruina, R. Tedrake and M. Wisse, "Efficient bipedal robots based on passive dynamic walkers," *Sci Mag* **307**, 1082–1085 (2005).
7. M. D. Mann, *The Nervous System and Behavior*, (Harper and Row, Philadelphia, PA 1981).
8. Y. Fukuoka, H. Kimura and A. H. Cohen, "Adaptive dynamic walking of a quadruped robot on irregular terrain based on biological concepts," *Int J Robot Res* **22**(3–4) 187–202 (2003).
9. J. Nakanishi, J. Morimoto, G. Endo, G. Cheng, S. Schaal and M. Kawato, "Learning from demonstration and adaptation of biped locomotion," *Robot Autonom Syst* **47**, 79–91 (2004).
10. J. Morimoto, G. Cheng, C. G. Atkeson and G. Zeglin, "A Simple Reinforcement Learning Algorithm for Biped Walking," *Proceedings of IEEE International Conference on Robotics and Automation*, **3** (Apr. 2004) pp. 3030–3035.
11. M. Vukobratovic and B. Borovac, "Zero moment point—Thirty five years of its life," *Int J Humanoid Robot* **1**(1), 157–173 (2004).
12. J.-H. Kim, D.-H. Kim, Y.-J. Kim, K.-H. Park, J.-H. Park, C.-K. Moon and K. T. Seow, "Humanoid Robot HanSaRam: Schemes for ZMP Compensation," *Proceedings of International Conference on Computational Intelligence, Robotics and Autonomous Systems*, (2003).
13. J. Vermeulen B. Verrelst, D. Lefeber P. Kool and B. Vanderborght, "A real-time joint trajectory planner for dynamic walking bipeds in the sagittal plane," *Robotica* **23**(6), (2005), pp. 669–680.
14. R. Zhang, P. Vadakkepat and C. M. Chew, "Motion Planning for Biped Robot Climbing Stairs ," *Proceeding of FIRA Robot World Congress*, Vienna, Austria (Oct 1–3, 2003).
15. K. Hirai, M. Hirose, Y. Haikawa and T. Takenaka, "The Development of Honda Humanoid Robot," *Proceedings of the 1998 IEEE International Conference on Robotics and Automation*, 1321–1326 (1998).
16. H.-O. Lim, Y. Kaneshima and A. Takanishi, "Online Walking Pattern Generation for Biped Humanoid Robot with Trunk," *Proceedings of IEEE International Conference on Robotics and Automation*, **3**(11–15), 3111–3116 (2002).
17. J. Yamaguchi, E. Soga, S. Inoue and A. Takanishi, "Development of a Bipedal Humanoid Robot-Control Method of Whole Body Cooperative Dynamic Biped Walking," *Proceedings of 1999 IEEE International Conference on Robotics and Automation*, **1**(10–15), 368–374 (1999).
18. K. Mitobe, G. Capi and Y. Nasu, "Control of walking robots based on manipulation of the zero moment point," *Robotica* **18**(6), (2000) pp. 651–657.
19. S. Kajita, F. Kanehiro, K. Kaneko, K. Fujiwara, K. Harada and K. Yokoi, Hirukawa, "Biped walking pattern generation by using preview control of zero-moment point," *Proceeding of IEEE International Conference on Robotics and Automation*, **2** (Sep. 14–19 2003) pp. 1620–1626.
20. J. H. Park and H. Chung, "ZMP compensation by online trajectory generation for biped robots," *Proceedings of IEEE International Conference on Robotics and Automation*, (Oct 10–15 1999) **4** pp. 960–965.
21. M. Shimojo, T. Araki, A. Ming and M. Ishikawa, "A ZMP sensor for a biped robot," *Proceedings 2006 Conference on International Robotics and Automation* (2006), pp. 1200–1205.
22. M. Vukobratović, B. Borovac, D. Surla and D. Stokić, *Biped Locomotion: Dynamics, Stability, Control and Application*, (Berlin, Germany, Springer-Verlag, 1990).
23. C. E. Bauby and A. D. Kuo, "Active control of lateral balance in human walking," *J. Biomech.* **33**, 1433–1440 (2000).